

Signal-to-noise ratio, error and uncertainty of PIV measurement

Zhenyu Xue¹, John J. Charonko² and Pavlos P. Vlachos³

¹ Department of Mechanical Engineering, Virginia Tech, Blacksburg, Virginia
conanxzy@vt.edu

² Department of Mechanical Engineering, Virginia Tech, Blacksburg, Virginia
jcharonk@vt.edu

³ Department of Mechanical Engineering, Virginia Tech, Blacksburg, Virginia
pvlachos@vt.edu

ABSTRACT

In particle image velocimetry (PIV) the measurement signal is contained in the recorded intensity of the particle image pattern superimposed on a variety of noise sources. The inherent amount of signal mutual information between consecutive images governs the strength of the resulting PIV cross correlation and ultimately the accuracy and uncertainty of the produced PIV measurements. Hence we posit that correlation signal-to-noise-ratio (SNR) metrics calculated from the correlation plane can be used to quantify the quality of the correlation and the resulting uncertainty of an individual measurement. In this paper we present a framework for evaluating the correlation SNR using a set of different metrics, which in turn are used to develop models for uncertainty estimation. A new SNR metric termed “mutual information” (MI) which quantifies the amount of common information (particle pattern) between two consecutive images is also introduced and investigated. This measure provides a direct estimation of the apparent $N_I F_I F_O$ parameter of an image pair providing an alternative approach towards uncertainty estimation but also connecting the current development to one of the most fundamental principles of PIV and the previously established theory. The SNR metrics and corresponding models presented herein are expanded to be applicable to both standard and filtered correlations and the notion of “valid” measurement is redefined with respect to the correlation peak width. These advancements lead to more robust uncertainty estimation models, which are tested against both synthetic benchmark data as well as actual experimental measurements. For all cases considered here, expanded uncertainties are estimated at the 95% confidence level, and the resulting calculated coverages are approximately 95% thus demonstrating the feasibility and applicability of these new models for direct estimation of uncertainty for individual PIV measurements.

1 Introduction

Particle Image Velocimetry (PIV) is a non-invasive, quantitative, flow visualization tool developed to measure fluid velocities over a wide range of length and time scales. The technique typically employs micron-size flow tracer particles, which are illuminated by a pulsed laser and imaged with a high-frequency camera. Processing algorithms are then used to determine the displacement of particle patterns within an image sequence and to estimate the velocity field [1]. An overview of the development of DPIV over the first 20 years of the method is given by Adrian [2].

PIV was first developed in the 1980s, and the initial work of Meynart [3] was followed by numerous seminal contributions that established the foundations of the method [4-7]. The introduction of digital image acquisition [1] (DPIV) provided a transformative evolution of the method and triggered its widespread use and an explosive growth of applications. Refinements over the next 20 years improved robustness and accuracy of the technique, including the development of stereoscopic (3-component) planar PIV [8, 9], iterative, and adaptive methods [10-14]. A

comprehensive history of these improvements can be traced through early reviews [7, 15] and more recent sources [2, 16-18]. Currently, the term PIV is used to encompass the extensive family of methods that are based on evaluating the particle patterns displacement using statistical cross-correlation of consecutive images with high number density of flow tracers [16].

However, the development of PIV methods did not involve simultaneous rigorous quantification of measurement uncertainty. As a result, despite the numerous applications, theory, and contributions, there is currently no widely accepted framework for reliable quantification of PIV measurement uncertainty. The situation is exacerbated by the fact that PIV measurements involve instrument and algorithm chains with coupled uncertainty sources, rendering quantification of uncertainty far more complex than most measurement techniques. Consequently PIV results are often received with skepticism. Therefore developing a fundamental methodology for quantifying the uncertainty for PIV is an important and outstanding challenge.

The first attempt to tackle this problem employed an “error-surface” methodology which would be constructed by mapping the effects of selected primary error sources such as shear, displacement, seeding density, and particle diameter to the true error for a given measurement [19]. This approach is roughly analogous to a more traditional instrument calibration procedure for standard experimental instruments. The generated error surface provides the means to associate the corresponding distribution of errors to any combination of inputs of the error sources within their parameters space, as quantified directly from the actual experiment. Ultimately in order to comprehensively quantify the uncertainty, all possible combinations of displacements, shears, rotations, particle diameters, and any other parameter used must be exhaustively tested which can make this method computationally expensive. Moreover, many of the relevant parameters may not be easily obtained from a real experiment.

Sciacchitano et al. proposed a method to quantify the uncertainty of PIV measurement based on image matching [20]. The uncertainty of measured displacement is calculated from the ensemble of disparity vectors, which are due to incomplete match between particles, within the interrogation window. This method accounts for random and systematic errors, however peak-locking errors and truncation errors cannot be detected. Moreover to calculate the instantaneous local uncertainty, researchers need to do particle image pair detection and image matching for every single interrogation spot which makes this method also computationally expensive.

In this work we adopt an alternative approach and we seek to quantify the PIV displacement uncertainty directly from the information contained within the cross-correlation plane. The cross-correlation plane represents the distribution of probabilities of all possible particle image pattern displacements between consecutive frames, combined with the effect of the number of particles, the mean particle diameter and effects that contribute to loss of correlation. As described by Adrian and Westerweel [21] (p. 322): “*The height of the peak is proportional to the image density N_i , the out of plane loss of correlation F_O and the in-plane loss of correlation F_I . The shape of the peak is determined by the convolution of the particle image self correlation with the displacement distribution in the measurement volume.*” In other words, the correlation plane is a surrogate of the combined effects of the various sources of error that govern the accurate estimation of a particle pattern displacement. Hence, in this work we will seek to establish appropriate measures that quantify the cross-correlation quality by means of signal-to-noise ratio (SNR) and establish the relationship of these metrics to the individual measurement uncertainty.

One measure of the cross-correlation SNR is the primary peak ratio (PPR), namely the ratio between the highest correlation peak to the second tallest peak as shown in Figure 1. In early PIV papers, PPR was used as a measure of the detectability of the true displacement [22, 23]. A measurement would be considered as valid if PPR were higher than a user defined threshold (often 1.2), or the measurement is rejected if PPR is smaller than that value. Based on this criterion, it was established that the product of $N_i F_I F_O$ would determine the probability of getting a valid detection and in order to get a 95% probability of valid detection, the minimum $N_i F_I F_O$ value should be approximately 5 [24]. Unfortunately, the effects of in-plane and out-of-plane loss of correlation are difficult to quantify in real experiment,

thus making $N_I F_I F_O$ difficult to estimate in real experiment cases. However this establishes a clear relationship between a measure of the correlation strength (PPR) and number of correlated particle image pairs.

The PPR value is easy to compute and provides a practical measure of the quality of a cross-correlation. Hain and Kahler [25] suggest that a threshold PPR value of about 2 can reliably avoid spurious vectors, and based on this they proposed a scheme for the optimal selection of cross-correlations across a range of interframe time delays. Similarly for extending the PIV velocity dynamic range using multiple pulse separation imaging, Persoons and O'Donovan used a weighted peak ratio value as a criterion to calculate the optimum pulse separation [26].

Recently, Charonko and Vlachos proposed an uncertainty quantification method based on PPR [27]. The relationship between the distribution of velocity error and PPR value was studied and a model for calculating the uncertainty based on the PPR value of a given measurement was developed. Using this method, the uncertainty of PIV measurement can be predicted without the *a-priori* knowledge of image quality and local flow condition. Reliable uncertainty estimation results using a phase-filtered correlation [28-30] were shown. However for standard cross-correlation techniques, the uncertainty estimation provided by this method is not as good. This was attributed to the insufficient treatment of noise effects inherent in the standard cross-correlation.

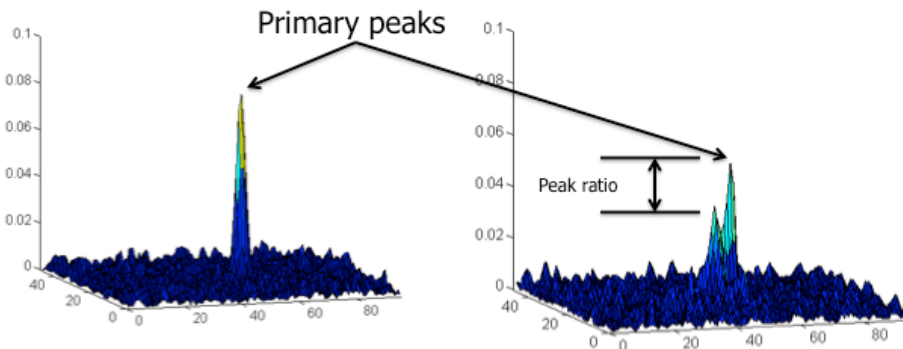


Figure 1: Left: Single cross-correlation peak with high probability of accurate detection. Right: Two primary peaks in the correlation plane. The closer the peak heights are with respect to each other, the lower the probability of accurate detection.

Beyond the PPR other metrics exist for quantifying the cross-correlation SNR. Kumar and Hassebrook defined several signal to noise ratios of the correlation related to peak detectability, namely peak ratio (PPR), peak-to-root mean square ratio (PRMSR), and peak-to-correlation energy (PCE) [31]. All three of these metrics measure the strength of correlation but the PPR is a mostly heuristic parameter while in contrast the PCE and PRMSR are more fundamental rooted to signal processing theory [31]. However, within the scope of PIV methods, neither PCE nor PRMSR have been considered.

In this work, we will extend the original work by Charonko and Vlachos [27] to calculate cross-correlation SNR metrics using only the information from the correlation plane to develop models for uncertainty estimation. Here, in addition to the PPR, we will consider PRMSR and PCE and cross-correlation entropy (based on information entropy [32]) and we expand the previous work to make these measures applicable to both standard and phase filtered cross-correlation. More importantly, we develop a new metric we term “mutual information” (MI) that we hypothesize provides a direct estimation of the apparent $N_I F_I F_O$ for each image pair. This metric also will be used to develop a model for uncertainty estimation but in contrast to the other models that are adopted from the generic signal processing literature, MI directly connects to the fundamental PIV principles.

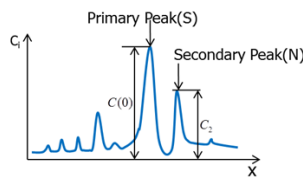
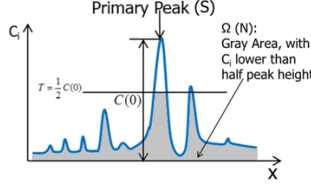
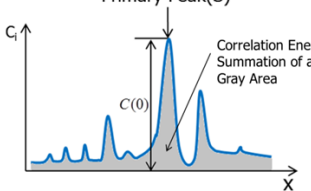
Details of the definition and calculation of these metrics will be provided in the following section. The relationship between velocity error distribution or standard uncertainty and each metric are obtained by statistical analysis. The functions used to quantify each relationship are calculated from curve fittings.

1. Background and Methodology

1.1. Correlation plane signal to noise ratio (SNR)

The random correlation peaks distributed along the correlation plane correspond to correlations between distinct particle image pairs. A valid displacement measurement is achieved when the highest detectable peak in the plane represents the true displacement. As a result, the strength (detectability) of the primary peak with respect to surrounding peaks represents the signal to noise ratio of the correlation plane. Hence following the work by Kumar and Hassebrook [31], measures of the correlation SNR can be defined and are shown in Table 1. These include the PPR, PRMSR, and PCE. Table 1 also provides the definitions of these filters and a one-dimensional graphical representation.

Table 1: Definition, separate parts and 1-D example of PPR, PRMSR and PCE

	Peak Ratio	Peak to Root Mean Square Ratio	Peak to Correlation Energy
Expression	$PPR = \frac{C_{\max}}{C_2}$	$PRMSR = \frac{ C_{\max} ^2}{C_{rms}^2}$	$PCE = \frac{ C_{\max} ^2}{E_c}$
Signal Part (S)	Primary Peak Height C_{\max}	Square Primary Peak Height $ C_{\max} ^2$	Square Primary Peak Height $ C_{\max} ^2$
Noise Part (N)	Secondary Peak Height C_2	Root Mean Square $C_{rms} = \left[\frac{1}{N} \sum_{i \in \Omega} C(i) ^2 \right]^{1/2}$	Correlation Energy $E_c = \int_{-\infty}^{\infty} C(x) ^2 dx$
Example (1D)			

Effectively all three of these metrics measure the detectability of the primary peak with respect to alternative correlations. However, in contrast to the PPR which is an ad-hoc metric, the PRMSR and PCE are amenable to analytical derivation if the signal statistical properties are known [31], hence they offer the potential for developing a corresponding theoretical foundation for the uncertainty estimation. This aspect however will not be pursued during this work.

Another signal to noise ratio measure considered herein is the cross-correlation entropy or information entropy [32]. This is based on the notion that if perfect matching between two image patterns exists in the absence of any noise, the correlation will yield a single sharp peak and the correlation entropy will be minimum. As more random correlations exist the entropy would increase. To calculate the entropy of the cross correlation plane, we first construct the histogram of the correlation plane based on the correlation value of every point on the plane. In our work, we use 30 bins to build the histogram. After the histogram is made, the probability of finding one point in a certain bin is calculated as:

$$p_i = \frac{\text{\# of points @ bin } i}{\text{Total \# points of whole plane}}$$

Then the entropy of the cross correlation plane was calculated as:

$$Entropy = \sum_{i=1}^{30} p_i \log 1/p_i = -\sum_{i=1}^{30} p_i \log p_i \quad (1)$$

1.2. Role of image background noise on correlation SNR

The information about the true displacement in the correlation plane is contained in the correlation of the fluctuating intensities. If the correlation is written as:

$$R(s,t) = R_C(s,t) + R_F(s,t) + R_D(s,t) \quad (2)$$

where the overall correlation plane is decomposed into R_C , R_F and R_D which are respectively the correlation of the mean background intensity over the interrogation windows, the correlation of the background noise in one window with the fluctuating intensity in the other window, the cross correlation of the fluctuating image intensities. It is common practice to subtract the image mean intensity before performing a cross-correlation, which would effectively remove all contributions from the background and only provide R_D . However in practice this does not always hold true due to various illumination effects and imaging distortions. Although for the estimation of the true displacement such residuals would have negligible effect, in contrast for the calculation of the correlation SNR they can profoundly affect the metrics. In the work by Charonko and Vlachos [27] the standard correlation which was subject to this effect performed inferiorly to the phase filter correlation which in turn is largely immune to such effects. Hence in order to address this limitation and provide more robust estimation of the different correlation metrics we propose that it is appropriate to subtract the minimum value of the correlation plane. This is demonstrated below.

Figure 2a and b shows an example of a particle image with and without background noise. The cross correlation plane of these two image sets are shown in Figure 3a and b. The minimum correlation value of the cross correlation plane is on the order of 10^6 . After we subtract the correlation plane of Figure 3b (R_D) from Figure 3a (R), the left plane Figure 3c can be considered as the correlation related to background image noise, the R_N term. The mean value of this plane is also close to 10^6 . Subtraction of the minimum correlation value from the correlation plane effectively eliminates the effect of background image noise on the cross correlation plane.

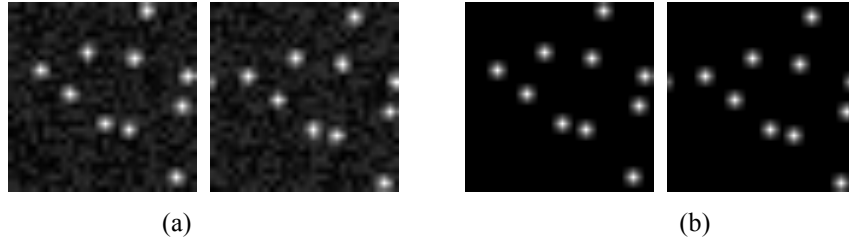


Figure 2: Particle image sets examples (a) with background noise; (b) same particle images without background noise

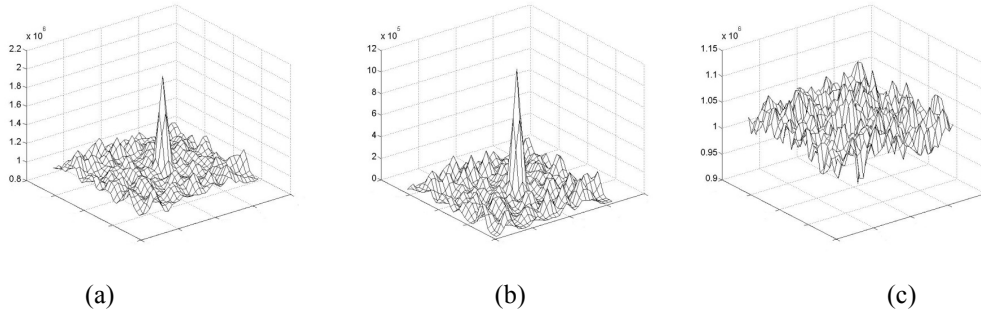


Figure 3: (a) cross correlation plane of particle images with background noise (b) cross correlation plane of particle images without background noise (c) the correlation plane related to background noise

1.3. Mutual Information (MI) and relationship to $N_1F_1F_0$

As discussed earlier, the correlation peak height is proportional to the product of the image density N_1 , the out of plane loss of correlation F_0 and the in-plane loss of correlation F_1 , and the shape of the peak is determined by the particle image self correlation and displacement distribution. Based on this insight we introduce a new measure of the correlation SNR which we term Mutual Information (MI). MI is defined as:

$$\frac{\text{Contribution of all correlated particle pairs}}{\text{Contribution of one correlated particle pair}} = \text{Total number of correlated particle pairs} = \text{Mutual information}$$

MI provides the means to directly calculate the $N_1F_1F_0$ from the information contained within the correlation plane. The calculation of the MI is based on dividing the peak magnitude of the cross-correlation by the autocorrelation of the “mean” particle as measured by the diameter of the image autocorrelation. A schematic of the calculation flow chart is shown below (Figure 4)

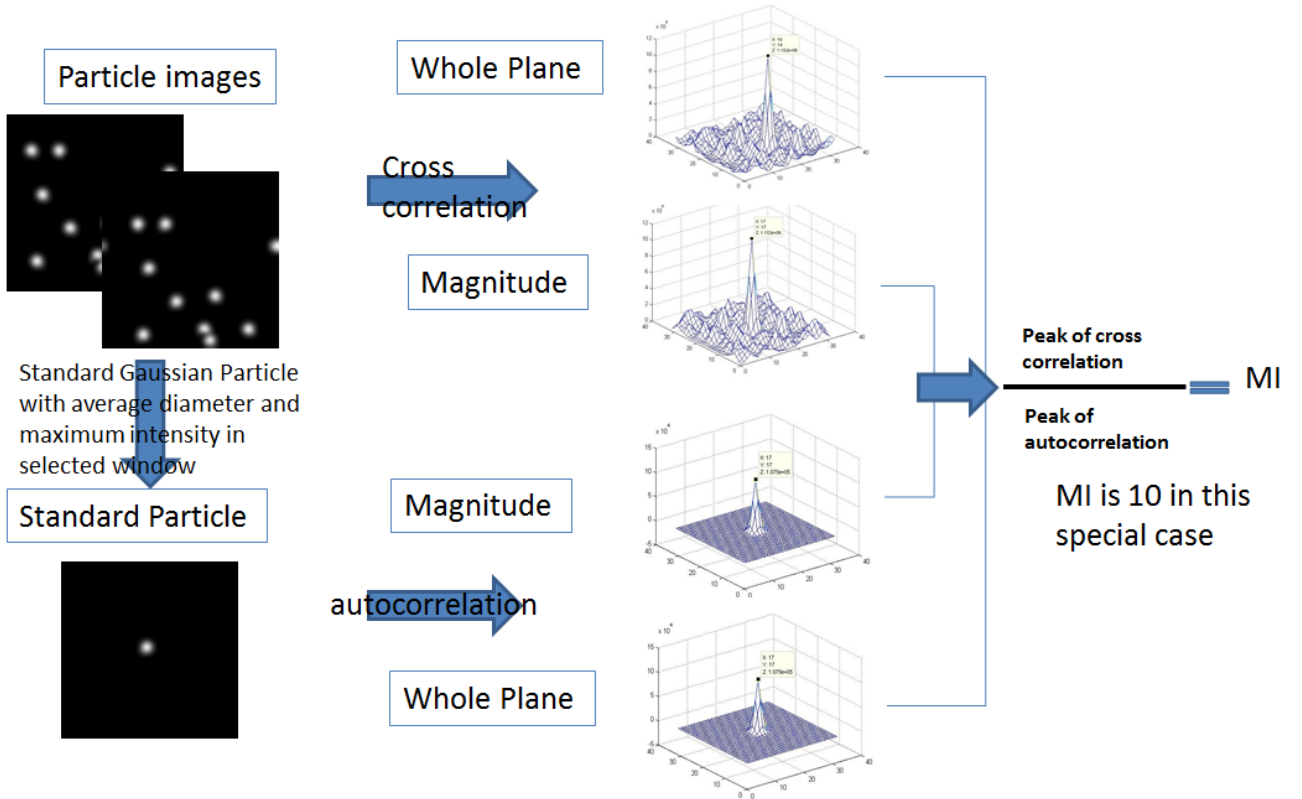


Figure 4: Schematic illustrating the calculation of MI

The image of one representative particle can be written as:

$$P(X, Y) = \iint J_0 e^{-8 \left(\frac{(X-X')^2}{d_0^2} + \frac{(Y-Y')^2}{d_0^2} \right)} \otimes \delta(X' - x_p, Y' - y_p) dX' dY' \quad (3)$$

where J_0 and d_0 are the intensity and diameter of the particle, x_p and y_p are the particle center coordinates. Then the autocorrelation can be calculated as:

$$A(s, t) = \iint P(X, Y) \times P(X+s, Y+t) dX dY \quad (4)$$

The autocorrelation peak height is the magnitude of autocorrelation plane:

$$A_0 = \frac{1}{16} J_0^2 d_0^2 \pi \quad (5)$$

We can write the analytical form of the cross correlation plane for image 1 and image 2 as:

$$R(s, t) = \iint I_1(X, Y) I_2(X + s, Y + t) dX dY \quad (6)$$

I_1 and I_2 are the expressions for image 1 and 2, with removing the background image noise effect we can consider the image as the summation of all particles within the window area:

$$I_1(X, Y) = \iint \sum_{p1} J_{i1} e^{-8\left(\frac{(X-X')^2}{d_{i1}^2} + \frac{(Y-Y')^2}{d_{i1}^2}\right)} \otimes \delta(X' - x_p, Y' - y_p) dX' dY' \quad (7)$$

$$I_2(X, Y) = \iint \sum_{p2} J_{i2} e^{-8\left(\frac{(X-X')^2}{d_{i2}^2} + \frac{(Y-Y')^2}{d_{i2}^2}\right)} \otimes \delta(X' - (x_p + \Delta x), Y' - (y_p + \Delta y)) dX' dY' \quad (8)$$

where p_1 and p_2 are the number of particles in image 1 and 2, J_i and d_i are the intensity and diameter of the i^{th} particle.

As mentioned before, the cross correlation peak can be considered as the summation of the autocorrelation of all correlated particles in both. By assuming the correlated particles in frame 1 and frame 2 are identical ($J_{i1} = J_{i2}$, $d_{i1} = d_{i2}$), we can show that the primary peak height of the cross correlation plane is:

$$\begin{aligned} C_{\max} &= \text{mag}\left(\sum_{p_c} \iint J_i^2 e^{-8\left[\frac{(X-x_p)^2}{d_i^2} + \frac{(Y-y_p)^2}{d_i^2}\right]} \times e^{-8\left[\frac{(X-x_p)^2}{d_i^2} + \frac{(Y-y_p)^2}{d_i^2}\right]} dX dY\right) \\ &= \sum_{p_c} \frac{1}{16} J_i^2 d_i^2 \pi \end{aligned} \quad (9)$$

where p_c is the number of correlated particles in both frames, J_i and d_i are the intensity and diameter of the i^{th} particle. Thus the number of correlated particle pairs or the amount of mutual information between consecutive frames (MI) can be estimated as:

$$MI = \frac{C_{\max}}{A_0} = \frac{\sum_{p_c} \frac{1}{16} J_i^2 d_i^2 \pi}{\frac{1}{16} J_0^2 d_0^2 \pi} = \sum_{p_c} \frac{\frac{1}{16} J_i^2 d_i^2 \pi}{\frac{1}{16} J_0^2 d_0^2 \pi} \quad (10)$$

It is clear then that in the case where every correlated particle has the same intensity and diameter as the reference particle ($J_i=J_0$, $d_i=d_0$), then MI will be equal to p_c . For interrogation regions where the particle size and brightness varies, the contribution of each particle will be proportionally weighted in terms of their effect on the final correlation signal.

1.4. Correlation width and valid measurements

The primary peak diameter can be calculated by [21]:

$$d_D = \sqrt{2d_\tau^2 + \frac{4}{3}a^2} \quad (11)$$

where d_r is the particle image diameter and a is a gradient parameter. But for given a correlation plane, the correlation peak width is usually calculated by performing a three-point Gaussian fit and then computing the diameter as 4 times the standard deviation for that Gaussian distribution. The location of the maximum value of that Gaussian distribution provides the sub-pixel displacement estimation for the PIV measurement. This is subject to the assumption that the true displacement is within the primary peak region. Thus, if the difference between the measured displacement and true displacement (error) is less than half of the peak diameter, the measurement should be considered as valid because the peak corresponds to the true displacement. However, previous works often use a fixed threshold value for detecting the failed measurement or outliers. Outliers are identified if the difference between the measured value and true value is larger than a pre-determined value, for example 0.5 or 1 pixel, regardless if the correct peak is detected or not. By using this criterion, the conventional definition of outliers is inconsistent with the notions of error and uncertainty. Namely, a wide peak at a location corresponding to the true displacement although it could yield errors in excess of 1 pixel, it would still be accurate but it will not be precise. Hence, using the traditional definition would inhibit the development of models for uncertainty quantification. Instead, we suggest that the criterion for a valid measurement should be based on the diameter of the correlation peak. If the error is less than half of the peak diameter, we conclude that the measurement successfully found the correct peak and it is indeed a valid measurement. Only those measurements providing the wrong primary peak are considered as invalid. An example of this “half peak diameter” criterion is shown in Figure 5. Note that the concepts of valid measurements versus outliers are different and distinct. An outlier is determined by statistical comparison with its neighbourhood while a valid or invalid measurement should be based on an independent assessment of the measurement’s success or failure, regardless of the statistical properties of the neighbourhood in which it is located. Using this model, a peak that has a width wider than a single pixel due to contributions of the particle size and a large shear gradient may be correctly identifying the velocity distribution within the interrogation region even if the highest point within that peak is located more than one pixel away from the velocity value at a location in the center of the correlated image. Thus, it should not be counted as a failure, but should be instead included as a valid measurement but with a larger than normal uncertainty.

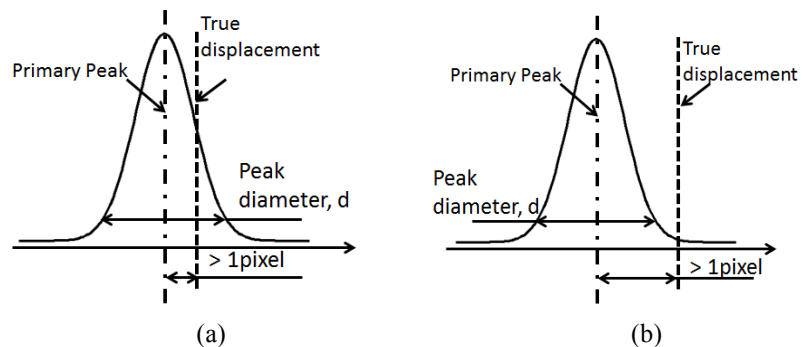


Figure 5: 1-D example of half peak diameter criterion (a) good measurement; (b) outlier

1.5. Synthetic image sets

Synthetic image sets with known displacements information were used to develop the relations between the uncertainty or error distribution and the measured metrics’ value.

1.5.1. Taylor vortex

The first data set is 100 image pairs of an ideal Taylor vortex flow field as was previously used by Charonko and Vlachos [27]. The vortex is located at the center of the image. The maximum circumferential velocity is $u_{\max} = 4$ pixels/frame at distance of $R_0 = 128$ pixels from the center. The velocity profile is given by:

$$u_{\theta}(r) = u_{\max} \frac{r}{R_0} \exp\left[\frac{1}{2}\left(1 - \frac{r^2}{R_0^2}\right)\right] \quad (12)$$

The image size is 1024X1024 pixels. Particles in the images are Gaussian with 3-pixel diameter at the 4 standard deviation level and had 8-bit intensity resolution. Seeding density is 20 particles per 32*32 pixel window on average.

1.5.2. Turbulent boundary layer

The second data set is 100 image pairs of turbulent boundary layer flow field (Case B of the Second International PIV challenge in 2003 [33]). The image quality is: 70 particles pairs per 32X32 region with 2.6 pixel average particle diameter at the 4 standard deviations.

1.5.3. Laminar separation bubble

The last data set is 18 image pairs of laminar separation bubble flow field (Case B of the Third International PIV Challenge in 2005 [34]). 25 particles per 32x32 window is the average seeding density of this data set. The average particle diameter is about 2.0 pixels.

1.6. Statistical analysis and Uncertainty estimation

After we got the value of metrics mentioned before and the error of all the vectors in the three synthetic image data sets, we divided all the data points into 40 bins based on the value of the calculated metrics. Previous work has shown that the difference between the absolute magnitudes of mean velocity error and absolute mean error plus the standard deviation was very small [35], justifying the continued use of the definition of $rms \delta_v$ from that work for the error distribution calculation. In each bin, the $rms \delta_v$ is calculated as:

$$rms \delta_{v,i} = \sqrt{mean(\delta_{v,i}^2)} = \sqrt{\frac{1}{N} \sum_{i=1}^N \delta_{v,i}^2} \quad (13)$$

where N is the number of data points in the i^{th} bin.

Measurement errors were first estimated at the standard uncertainty level, which should reflect one standard deviation level for the parent population of possible errors from which the true error on some measurement of the metric is drawn without respect of the exact shape of that distribution. The expanded uncertainty was calculated by making the assumption that all errors were drawn from normal distribution and the large sample assumption applied. We multiplied the standard uncertainty by a coverage factor, t_{CI} to get the expanded uncertainty. In this work we took $t_{95} = 2.0$, which means the true value of the measured quantity lies within a range bounded by the measured value plus or minus the expanded uncertainty (twice the standard uncertainty) 95% of the time. If the uncertainty model is correct, 95% of all data points will have a velocity error within the provided uncertainty range.

2. Result and discussion

2.1. Mutual information (MI)

As mentioned above, the MI is a more general form of $N_I F_I F_O$ combining the effects of particle intensity and diameter. To further prove the above idea, PIV standard image sets [36] were tested to show the relationship between MI and $N_I F_I F_O$. This data set was selected because in addition to the true velocity, the position and diameter of each particle in the image were also reported, which was necessary for a comparison between the two metrics. As mentioned before, different particles contribute differently in building the correlation plane, and thus the number of correlated particles ($N_I F_I F_O$) must be scaled by the particle intensity and diameter within each window. The result is shown in Figure 6. The X-axis shows the value of MI and the Y-axis shows the value of intensity scaled $N_I F_I F_O$. It is

clear that most of the results are aligned along the white dash line corresponding to $MI = N_I F_I F_O$ supporting the notion that the MI provides a direct estimate of the apparent $N_I F_I F_O$ for an individual image pair.

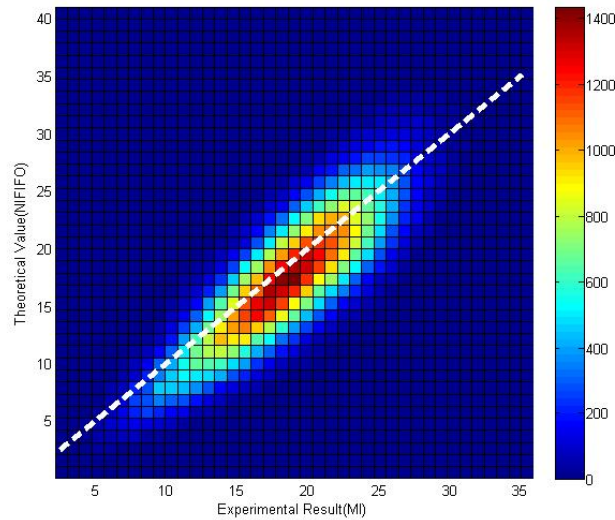


Figure 6: Mutual Information (MI) VS $N_I F_I F_O$. Color represents number of measurements in each bin.

The relationship between the mutual information and the distribution of velocity error for Case B of 2003 PIV Challenge using standard cross correlation method with 32X32 window size is shown in Figure 7. Details of statistical analysis and error distribution calculation are provided in [27]. The scatter plot shows all the combinations of MI and error. It is obvious that large errors are expected when the MI value is small. As shown in the plot, almost no measurement had both large error and high MI value in this special case. Moreover, MI shows a 95% valid detection probability for MI values larger than 5 which is consistent with previous findings for the valid vector detection probability versus $N_I F_I F_O$ [24]. When the MI value is below 5, the probability drops rapidly. This result further supports that MI and $N_I F_I F_O$ are measuring the same properties of the PIV experiment

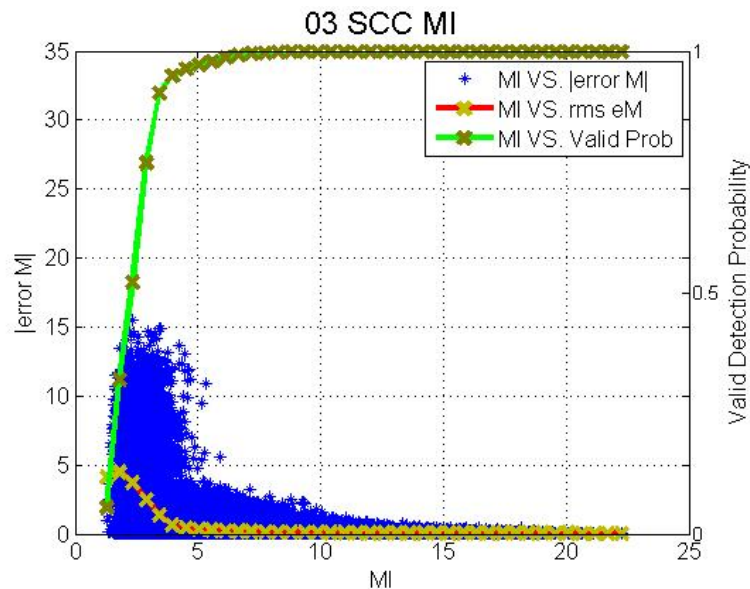


Figure 7: Plot of the distribution of velocity error using SCC processing versus correlation peak ratio for the turbulent boundary layer images of the 2003 PIV Challenge. (blue scatter dot) the measured distribution of MI value and error of velocity magnitude; (red line) mean error of velocity magnitude on each MI value; (green line) valid detection probability on each MI value.

2.2. Relationship of uncertainty versus cross-correlation SNR metrics

2.2.1. Uncertainty estimation model

The uncertainty model which provides a relationship between any of the SNR metrics to the standard uncertainty is based on a the fitting function proposed in [35]. Hence, the estimated standard uncertainty is calculated by determining the fitting parameters of the following equation:

$$u^2 = \left(M \exp \left(-\frac{1}{2} \left(\frac{\phi - N}{s} \right)^2 \right) \right)^2 + (A\phi^B)^2 + (C)^2 \quad (14)$$

The first term is a Gaussian function used to account for the uncertainty due to invalid measurements which contribute uncertainty M, where the exact value of M is related to the range of possible velocity measurements and the distribution of the true velocity within the sampled flow field [27]. The $(\phi - N)$ term allows the error to climb rapidly as the metric's value approaches some small number, and N is the theoretical minimum value of the calculated metric.

Based on the definition of each quantity, we can determine analytically what value of N we should use for each. For PPR, the minimum value is 1 when we have a primary peak and secondary peak with the same height. Based on the definition of PRMSR, when all points in C_{rms} have a value of half the main peak height the theoretical minimum value for PRMSR is 4. The extreme case for PCE occurs when the peak is only slightly higher than the rest of the correlation plane, and the rest of the plane shares the same correlation value; in this case the PCE value is close to 1. Because entropy behaves the opposite way as other basic SNR metrics, we take the inverse of entropy, i.e. $\phi = 1/\text{entropy}$ to keep the fitting function type consistent among all metrics. The theoretical minimum value for inverse entropy should be 0. The theoretical minimum value for MI is also 0 when no particles correlated between two consecutive image frames.

The second term in equation 14 is the contribution to the uncertainty by the valid vectors, which means the largest uncertainty that could be expected would be governed primarily by A if it can be assured that the given measurement is valid. The last term C is a constant, which corresponds to the lowest uncertainty we can achieve. The estimated uncertainty for a measurement with a given calculated metric value is governed by the combination of the above three terms.

Although outliers were detected by using the new half peak diameter rule described earlier, it is not appropriate to develop a model for uncertainty estimation using only the valid measurements. Unlike synthetic image sets, in real experiments the true velocity field is unknown and it is inevitable that velocity fields would be contaminated by invalid measurements. Therefore both invalid and valid vectors are included in developing the uncertainty model estimation. All three synthetic cases with 3 different window size (or effective window size for RPC method), 16X16, 32X32, and 64X64 were included in the test providing a sample containing 12 million data points.

2.3. Results of uncertainty estimation

In order to keep the calculation process consistent, we applied the minimum correlation value subtraction method as described earlier to both SCC and RPC. However, this method has a minimal effect on the RPC models since phase filtering is effectively immune to background noise effects. Figure 8 shows the curve fitting results for estimating the uncertainty using peak ratio with both RPC and SCC methods after the minimum subtraction. The corresponding curve fitting functions are:

$$u_{sc}^2 = \left(10.47 \exp \left(-\frac{1}{2} \left(\frac{PPR-1}{1.12} \right)^2 \right) \right)^2 + (1.913 PPR^{-1.371})^2 + 2.221e-14^2 \quad (15)$$

$$u_{rpc}^2 = \left(8.825 \exp \left(-\frac{1}{2} \left(\frac{PPR-1}{1.087} \right)^2 \right) \right)^2 + (1.642 PPR^{-1.01})^2 + 2.21e-14^2 \quad (16)$$

In the previously reported results for SCC processing, the fitted curve only partially agreed with the original data [35]. The current results shown in Figure 8a, show that the model fit provides agreement with the original data almost

across the whole range, with R square value of 0.98. The model for estimating uncertainty for SCC processing provides larger values by comparison to the RPC processing, but the relationships are now much more similar than they were in the previous work that did not use minimum subtraction. The green curves show the error distribution of velocity magnitude versus PPR of good vectors only.

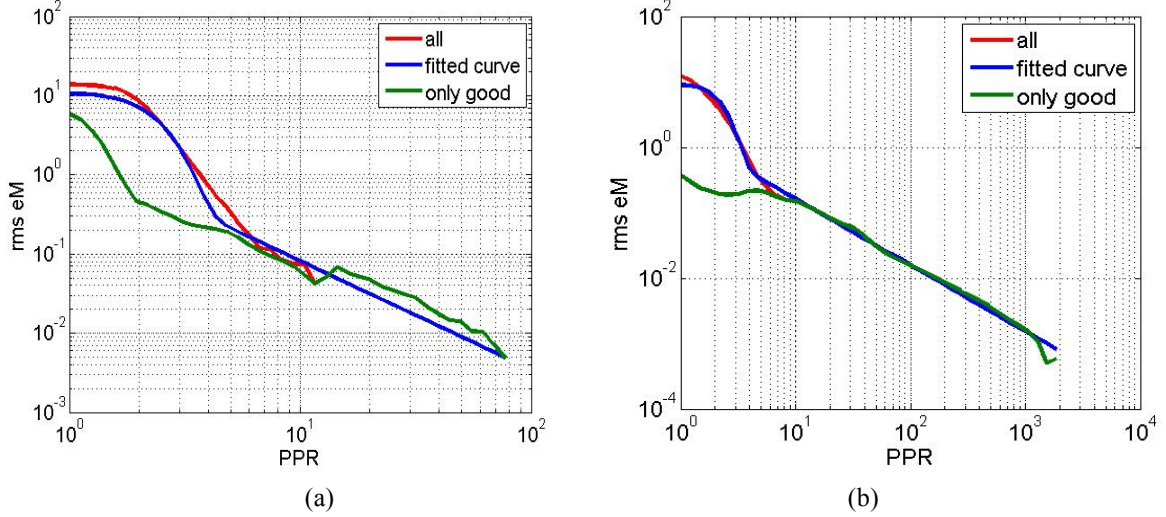


Figure 8: Plots of the relationship of the calculated standard uncertainty on velocity magnitude versus peak ratio for both the (a) SCC, and (b) RPC, for all three synthetic image sets. (red line) original curve of uncertainty on velocity magnitude versus peak ratio; (blue line) three term function fitted curve; (green line) uncertainty on velocity magnitude versus peak ratio for only valid vectors.

Figure 9-Figure 11 show the curve fitting results for estimating the uncertainty using other basic SNR metrics with both RPC and SCC methods. The fitting functions are:

$$u_{scc}^2 = \left((14.33 \exp(-\frac{1}{2}(\frac{PRMSR-4}{40.58})^2))^2 + (58.46 PRMSR^{-0.9939})^2 + 2.22e-14^2 \right) \quad (17)$$

$$u_{rpc}^2 = \left((9.88 \exp(-\frac{1}{2}(\frac{PRMSR-4}{99.19})^2))^2 + (40 PRMSR^{-0.7462})^2 + 2.221e-14^2 \right) \quad (18)$$

$$u_{scc}^2 = \left((15.36 \exp(-\frac{1}{2}(\frac{PCE-1}{27.71})^2))^2 + (23.27 PCE^{-0.8761})^2 + 2.221e-14^2 \right) \quad (19)$$

$$u_{rpc}^2 = \left((11.61 \exp(-\frac{1}{2}(\frac{PCE-1}{61.06})^2))^2 + (21.77 PCE^{-0.7353})^2 + 2.221e-14^2 \right) \quad (20)$$

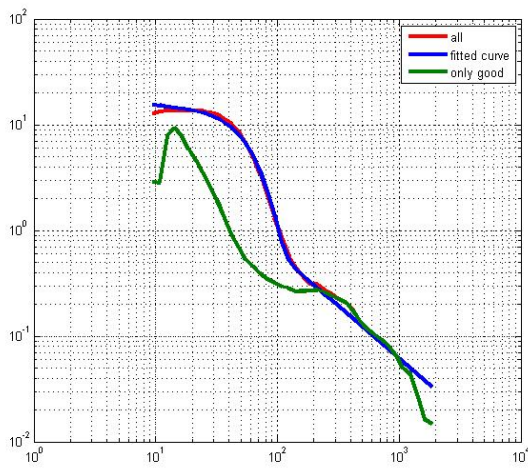
$$u_{scc}^2 = \left((80.64 \exp(-\frac{1}{2}(\frac{Entropy^{-1}}{0.4469})^2))^2 + (1.022 (Entropy^{-1})^{-2.232})^2 + 0.0122^2 \right) \quad (21)$$

$$u_{rpc}^2 = \left((26.19 \exp(-\frac{1}{2}(\frac{Entropy^{-1}}{0.7054})^2))^2 + (0.455 (Entropy^{-1})^{-0.4977})^2 + 2.241e-14^2 \right) \quad (22)$$

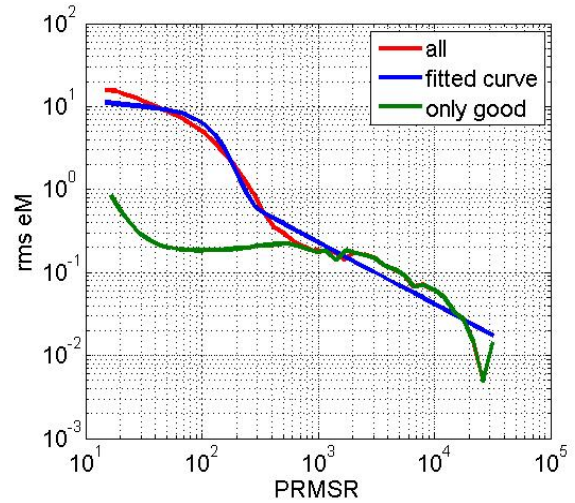
All these functions agree that the uncertainty would be larger for the SCC than the RPC for the same value of each metric. It is interesting to note that the maximum uncertainty predicted for PRMSR and PCE can be as large as 20 pixels even for valid measurements for both SCC and RPC methods. Despite the theoretical minimum value for PRMSR and PCE, in fact the PRMSR and PCE value is typically hundred times higher than the theoretical minimum value, so the uncertainty for valid vectors would never be that high for real cases. All these functions showed an acceptable agreement with the raw data, and the corresponding R^2 values for each function are shown in Table 2.

Table 2: R^2 vale of all fitting functions

	PPR	PRMSR	PCE	Entropy
SCC	0.98	0.99	0.99	0.98
RPC	0.99	0.97	0.95	0.92

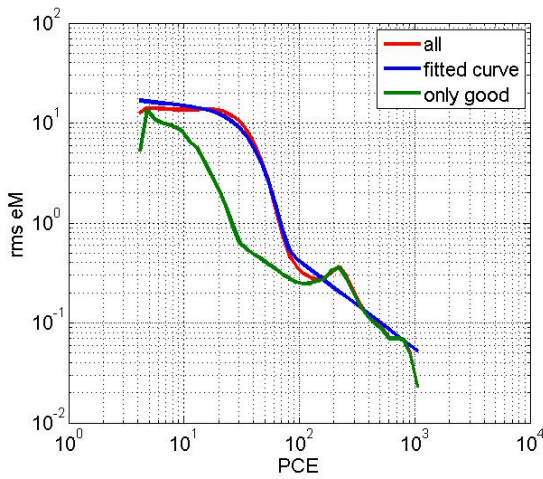


(a)

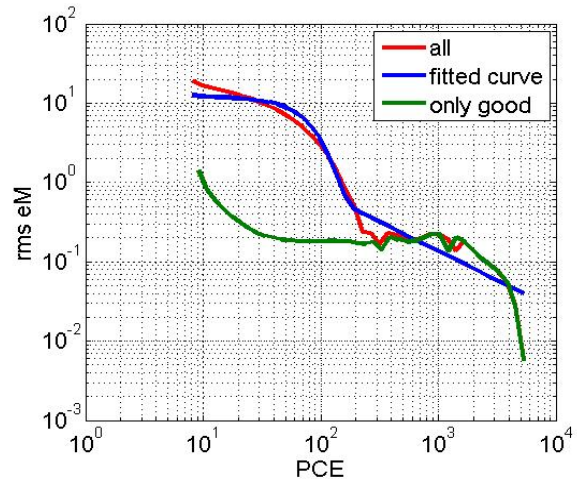


(b)

Figure 9: Plots of the relationship of the calculated standard uncertainty on velocity magnitude versus PRMSR for both the (a) SCC, and (b) RPC, for all three synthetic image sets. (red line) original curve of uncertainty on velocity magnitude versus PRMSR; (blue line) three term function fitted curve; (green line) uncertainty on velocity magnitude versus PRMSR for only valid vectors



(a)



(b)

Figure 10: Plots of the relationship of the calculated standard uncertainty on velocity magnitude versus PCE for both the (a) SCC, and (b) RPC, for all three synthetic image sets. (red line) original curve of uncertainty on velocity magnitude versus PCE; (blue line) three term function fitted curve; (green line) uncertainty on velocity magnitude versus PCE for only valid vectors

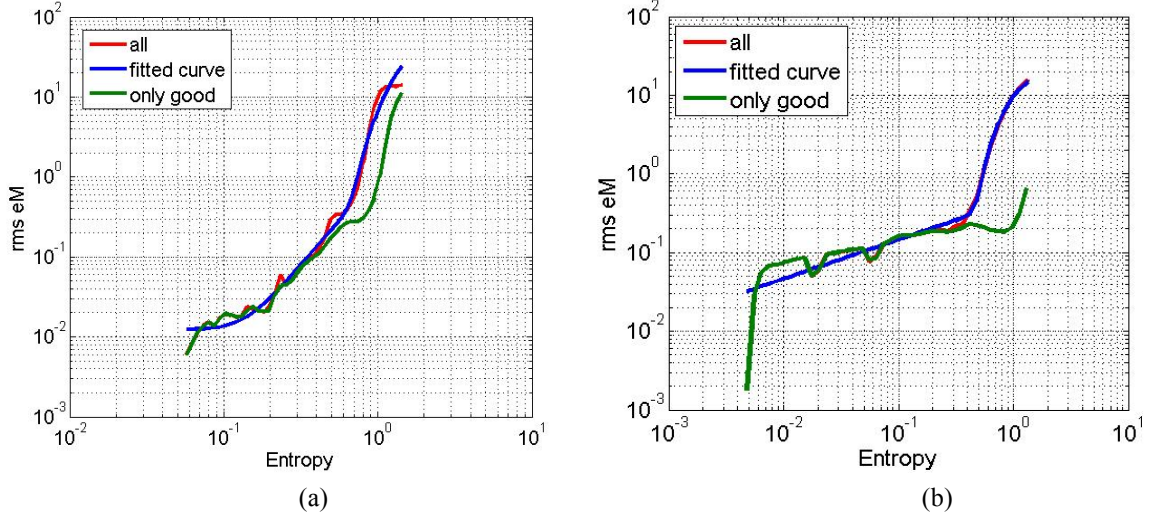


Figure 11: Plots of the relationship of the calculated standard uncertainty on velocity magnitude versus Entropy for both the (a) SCC, and (b) RPC, for all three synthetic image sets. (red line) original curve of uncertainty on velocity magnitude versus Entropy; (blue line) three term function fitted curve; (green line) uncertainty on velocity magnitude versus Entropy for only valid vectors

The curve fitting for MI was done using all three synthetic data sets with only 32X32 window size, as shown in Figure 10. The fitting functions are:

$$u_{scc}^2 = \left((26.22 \exp(-\frac{1}{2}(\frac{MI}{2.144})^2)) \right)^2 + (0.8739MI^{-0.9439})^2 + 0.05^2 \quad (23)$$

$$u_{rpc}^2 = \left((2.382 \exp(-\frac{1}{2}(\frac{MI}{2.056})^2)) \right)^2 + (0.3401MI^{-0.7386})^2 + (2.23e-14)^2 \quad (24)$$

The R^2 value is 0.99 for SCC model, and 0.98 for RPC model. The green curve shows the rms error of velocity magnitude only for valid vectors, which is almost linear in the logarithm domain. This fact further supports our assumption that the power-law term counts for uncertainty of valid measurements. It is interesting to note that the constant term in the SCC model is 0.05 pixels which matches well with the widely accepted value about the expected accuracy of PIV measurements under ideal (simulated) conditions [37]. The RPC function is similar to SCC with smaller error value. The curve for the RPC is not as smooth as the SCC one because in RPC processing the magnitude part of correlation which contains the particle image information is removed. As a result the MI value captures only the contribution of the loss of correlation and not the particle number density. This is a limitation of the current formulation that will be addressed in the future.

The above equations are used for estimating the standard uncertainty using the corresponding metrics. This standard uncertainty was then multiplied by a coverage factor of $t_{95}=2.0$ to yield an estimate of the uncertainty at the 95% confidence interval using the large sample approximation for a normal error distribution. Finally, the percent coverage of the expanded uncertainty was calculated in comparison to the exact true error for each velocity measurement according to the following formula:

$$\text{coverage} = \frac{\# \text{ of estimates for which } \delta_v \leq U_v}{\text{total \# of velocity estimates}} \times 100\% \quad (25)$$

The coverage should be close to 95% for the expanded uncertainty if the uncertainty estimation was correct on average. The exact values of coverage factor of all functions using all three synthetic data sets with 16X16, 32X32 and 64X64 window sizes (for MI, we use 32X32 window size only) are listed in Table 3. All of the coverage factors are very close to 95%.

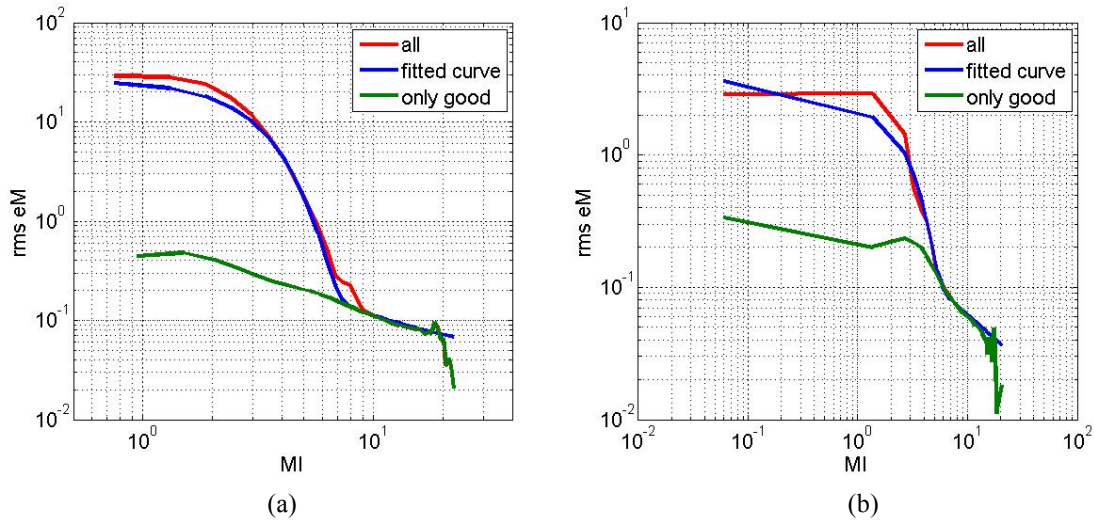


Figure 12: Plots of the relationship of the calculated standard uncertainty on velocity magnitude versus MI for both the (a) SCC, and (b) RPC, for all three synthetic image sets. (red line) original curve of uncertainty on velocity magnitude versus MI; (blue line) three term function fitted curve; (green line) uncertainty on velocity magnitude versus MI for only valid vectors

Table 3: Coverage vale of all fitting functions with synthetic data sets

	PPR	PRMSR	PCE	Entropy	MI
SCC	95.9%	95.6%	96.1%	95.4%	95.7%
RPC	94.9%	94.3%	94.7%	94.7%	96.0%

2.4. Application to real flow fields

Our uncertainty models were further tested with real experimental data. In this work, we are using the same data set of stagnation plate flow used by Charonko and Vlachos [27]. The experimental details can be found therein. The details of calculating the time average field and then the uncertainty introduced by the fitting process were also described in [27]. Afterwards the combined standard uncertainty from both PIV correlation and the experimental fit for the “true” field is multiplied by a factor of 2 to yield the expanded uncertainty U_{total} , and finally the coverage factor is calculated by the following formula:

$$\text{coverage} = \frac{\# \text{ of estimates for which } \delta_v \leq U_{total}}{\text{total \# of velocity estimates}} \times 100\% \quad (26)$$

The exact values of coverage factor of each function using the real experiment data set with 32X32 window sizes are listed in Table 3. Values of all coverage factors are close to 95%.

Table 4: Coverage vale of all fitting functions with real experiment sets

	PPR	PRMSR	PCE	Entropy	MI
SCC	95.2%	94.0%	96.1%	94.1%	95.4%
RPC	95.3%	95.1%	96.4%	94.7%	96.4%

3. Conclusion

In this paper, we show that cross-correlation SNR metrics calculated exclusively from the correlation plane can be used to estimate the uncertainty of the PIV measurements. In the first part of our work, metrics of basic correlation SNR related to the peak detectability are introduced. We also develop a new metric termed Mutual Information (MI) to estimate the real and apparent $N_I F_I F_O$ directly from the calculated correlation plane. Both theoretical derivation and experimental results support that MI corresponds to the apparent $N_I F_I F_O$ and would be a practical measure of the correlation SNR with direct connection to the established PIV theory. A simple but consequential correction on the correlation plane is introduced using a minimum correlation value subtraction to remove the effect of the background image noise and thus improve the model's performance for uncertainty estimation.

The relationship between the uncertainty and the metrics of correlation SNR of individual velocity measurements were explored using both robust phase correlation (RPC) and standard cross correlation (SCC) method. The standard uncertainty is governed by a well-defined relationship between the correlation SNR using both methods. This relation is quantified using a three-term formulation for both processing methods. In the three-term function, the Gaussian distribution term is related to probability of occurrence of invalid measurements; the power-law term describes the primary behavior of the uncertainty versus the metrics; and a constant expresses the minimum expected uncertainty level for the corresponding methodology, regardless of value of the metrics. The formulas successfully predicted the expanded uncertainty coverage close to 95% over all three synthetic image sets as well as a 2D stagnation point real experiment case using all provided metrics using both SCC and RPC method.

In conclusion, this paper provides a general framework of models for predicting the expected uncertainty levels for individual velocity measurement in a PIV flow field without the knowledge of local flow conditions using only the information contained in the calculated correlation plane. This work continues work establishing the foundations towards the growing understanding of PIV uncertainty estimation.

4. References

1. Willert, C.E. and M. Gharib, *Digital Particle Image Velocimetry*. Experiments in Fluids, 1991. **10**(4): p. 181-193.
2. Adrian, R.J., *Twenty years of particle image velocimetry*. Experiments in Fluids, 2005. **39**(2): p. 159-169.
3. R, M., *Mesure de champs de vitesse d'écoulements fluides par analyse de suites d'images obtenues par diffusion d'un feuillet lumineux*. Ph.D. thesis, 1983. **Faculté des Sciences Appliquées, Université Libre de Bruxelles**.
4. Yao, C.S. and R.J. Adrian, *Orthogonal Compression and 1-D Analysis Technique for Measurement of 2-D Particle Displacements in Pulsed Laser Velocimetry*. Applied Optics, 1984. **23**(11): p. 1687-1689.
5. Adrian, R.J. and C.S. Yao, *Pulsed Laser Technique Application to Liquid and Gaseous Flows and the Scattering Power of Seed Materials*. Applied Optics, 1985. **24**(1): p. 44-52.
6. Keane, R.D. and R.J. Adrian, *Optimization of Particle Image Velocimeters .1. Double Pulsed Systems*. Measurement Science & Technology, 1990. **1**(11): p. 1202-1215.
7. Adrian, R.J., *Particle-Imaging Techniques for Experimental Fluid-Mechanics*. Annual Review of Fluid Mechanics, 1991. **23**: p. 261-304.
8. Soloff, S.M., R.J. Adrian, and Z.C. Liu, *Distortion compensation for generalized stereoscopic particle image velocimetry*. Measurement Science & Technology, 1997. **8**(12): p. 1441-1454.
9. Willert, C., *Stereoscopic digital particle image velocimetry for application in wind tunnel flows*. Measurement Science & Technology, 1997. **8**(12): p. 1465-1479.
10. Scarano, F., *Iterative image deformation methods in PIV*. Measurement Science & Technology, 2002. **13**(1): p. R1-R19.
11. Scarano, F., *Theory of non-isotropic spatial resolution in PIV*. Experiments in Fluids, 2003. **35**(3): p. 268-277.

12. Scarano, F., *A super-resolution particle image velocimetry interrogation approach by means of velocity second derivatives correlation*. Measurement Science & Technology, 2004. **15**(2): p. 475-486.
13. Wereley, S.T. and L. Gui, *A correlation-based central difference image correction (CDIC) method and application in a four-roll mill flow PIV measurement*. Experiments in Fluids, 2003. **34**(1): p. 42-51.
14. Wereley, S.T. and C.D. Meinhart, *Second-order accurate particle image velocimetry*. Experiments in Fluids, 2001. **31**(3): p. 258-268.
15. Grant, I., *Particle image velocimetry: A review*. Proceedings of the Institution of Mechanical Engineers Part C-Journal of Mechanical Engineering Science, 1997. **211**(1): p. 55-76.
16. Adrian, R.J. and J. Westerweel, *Particle Image Velocimetry*. 2010: Cambridge Univ Pr. 558.
17. Kompenhans, J., et al., *Particle image velocimetry. a practical guide ; with 42 tables*. 2007. 448.
18. Stanislas, M., J. Kompenhans, and J. Westerweel, *Particle image velocimetry. progress towards industrial application*. 2000: Kluwer Academic Pub. 540.
19. Timmins, B., et al., *A method for automatic estimation of instantaneous local uncertainty in particle image velocimetry measurements*. Experiments in Fluids, 2012. **53**(4): p. 1133-1147.
20. Sciacchitano, A., B. Wieneke, and F. Scarano, *PIV uncertainty quantification by image matching*. Measurement Science and Technology, 2013. **24**(4): p. 045302.
21. Adrian, R.J. and J. Westerweel, *Particle Image Velocimetry*. 2011, Cambridge; New York: Cambridge University Press.
22. Keane, R.D. and R.J. Adrian, *Optimization of particle image velocimeters. I. Double pulsed systems*. Measurement Science and Technology, 1990. **1**(11): p. 1202.
23. Keane, R.D. and R.J. Adrian, *Optimization of particle image velocimeters: II. Multiple pulsed systems*. Measurement Science and Technology, 1991. **2**(10): p. 963.
24. Keane, R. and R. Adrian, *Theory of cross-correlation analysis of PIV images*. Applied Scientific Research, 1992. **49**(3): p. 191-215.
25. Hain, R. and C.J. Kahler, *Fundamentals of multiframe particle image velocimetry (PIV)*. Experiments in Fluids, 2007. **42**(4): p. 575-587.
26. Persoons, T. and T.S. O'Donovan, *High Dynamic Velocity Range Particle Image Velocimetry Using Multiple Pulse Separation Imaging*. Sensors, 2010. **11**(1): p. 1-18.
27. Charonko, J.J. and P.P. Vlachos, *Estimation of uncertainty bounds for individual particle image velocimetry measurements from cross-correlation peak ratio*. Measurement Science and Technology, 2013. **24**(6): p. 065301.
28. Eckstein, A. and P.P. Vlachos, *Digital particle image velocimetry (DPIV) robust phase correlation*. Measurement Science and Technology, 2009. **20**(5): p. 055401.
29. Eckstein, A. and P.P. Vlachos, *Assessment of advanced windowing techniques for digital particle image velocimetry (DPIV)*. Measurement Science and Technology, 2009. **20**(7): p. 075402.
30. Eckstein, A.C., J. Charonko, and P. Vlachos, *Phase correlation processing for DPIV measurements*. Experiments in Fluids, 2008. **45**(3): p. 485-500.
31. Kumar, B.V.K.V. and L. Hassebrook, *Performance measures for correlation filters*. Appl. Opt., 1990. **29**(20): p. 2997-3006.
32. Shannon, C.E., *A mathematical theory of communication*. SIGMOBILE Mob. Comput. Commun. Rev., 2001. **5**(1): p. 3-55.
33. Stanislas, M., et al., *Main results of the Second International PIV Challenge*. Experiments in Fluids, 2005. **39**(2): p. 170-191.
34. Stanislas, M., et al., *Main results of the third international PIV Challenge*. Experiments in Fluids, 2008. **45**(1): p. 27-71.

35. Adric, E. and P.V. Pavlos, *Digital particle image velocimetry (DPIV) robust phase correlation*. Measurement Science and Technology, 2009. **20**(5): p. 055401.
36. Okamoto, K., et al., *Evaluation of the 3D-PIV Standard Images (PIV-STD Project)*. Journal of Visualization, 2000. **3**(2): p. 115-123.
37. Huang, H., D. Dabiri, and M. Gharib, *On errors of digital particle image velocimetry*. Measurement Science and Technology, 1997. **8**(12): p. 1427.